Discontinuity Model for Internal Transport Barrier Formation in Reversed Magnetic Shear Plasmas

Y. Kishimoto, J-Y. Kim†, W. Horton*, T. Tajima*, M.J. LeBrun*

Japan Atomic Energy Research Institute, Naka Fusion Research Establishment
Naka, Ibaraki, 311-01 Japan
† Korea Basic Science Institute, 52 Yeoeundong, Yusung, Korea
*Institute for Fusion Studies, The University of Texas at Austin, Austin, Texas, 78712 USA

To aid in understanding the internal transport barrier (ITB) being formed in reversed magnetic shear experiments, in addition to the well known shear flow effect, we point out an important *nonlocal effect* and/or *finite size effect* which comes from the complex behavior of the nonlocal mode over a finite radial region around the minimum q(safety factor)-surface. The nonlocal mode changes its structure depending on the sign of the magnetic shear and due to this fact, the nonlocal modes are weakly excited across the q_{min}-surface. This leads to a *discontinuity* or *gap* which disconnects the phase relation in the global wave structure across the q_{min}-surface. Once such a discontinuity (or gap) is formed, transport suppression occurs and therefore a transport barrier can be expected near the q_{min}-surface. We confirm the existence of this discontinuity using a toroidal particle simulation.

1 INTRODUCTION

The turbulent structure of drift waves in a toroidal geometry is becoming clearer due to recently developed toroidal simulations [1-4] and theory [5-6]. According to these analyses, the linear drift waves in a toroidal geometry form a radially extended nonlocal structure whose width Δr is approximately given by

$$\Delta r \simeq (\rho_i L/\hat{s})^{\alpha}, \quad \text{with} \quad \alpha \simeq 0.5 \tag{1}$$

i.e. the geometrical mean between the ion Larmor radius ρ_i and the equilibrium scale length L (such as $L \sim a$: plasma minor radius or $L \sim L_T \equiv -(\partial \ln T_i/\partial r)^{-1}$: ion temperature scale length). Here, $\hat{s}[\equiv r(d\ln q/dr)]$ represents the local magnetic shear for a given safety factor $q(r)$. Although the mode width is affected by the plasma rotation, the results suggest that *nonlocal effect* and/or *finite size effect* of the plasma are important to understand various transport properties. Among them, the internal transport barrier (ITB) observed in a reversed magnetic shear configuration shows remarkable features and has been widely studied. Since the nonlocal modes sensitively depend on the magnetic structure, it is essential to know how the nonlocal modes behave in weak and/or reversed magnetic shear plasma.

In the paper, we investigate the drift waves [mainly the ion temperature gradient (ITG) mode] in such circumstances using a theory and a toroidal particle code. At first, we describe the 2-dimensional (2D) mode structure in toroidal geometry based on our theory [6] and discuss how the modes are influenced by the change of magnetic shear and by the plasma shear flow. The theoretical aspects in a weak magnetic shear plasma are compared with the simulation results. In a reversed q-profile, since the magnetic shear becomes extremely weak around the minimum q surface (hereafter q_{min}-surface) and changes its sign, the effect of the toroidal coupling is weakened and the nonlocal modes are weakly excited. This leads to an idea of the formation of a *discontinuity* (or *gap*) which disconnects the phase relation of the modes excited inside and outside the q_{min}-surface. Once such a discontinuity is formed, the transport suppression and therefore the transport barrier can be expected near the q_{min}-surface. To check the above hypothesis, we perform a toroidal simulation with a reversed q-profile.

In Sec.2, we present a theory for 2D drift wave structure and discuss the properties. The ITG modes in the reversed magnetic shear plasma is discussed in Sec.3 and numerical results are presented in Sec. 4. Concluding remarks are added in Sec.6.

2 Two Dimensional Toroidal Drift Wave Structure

2.1 Theory of 2D drift wave structure and characteristics

Here, we expand the drift wave eigen-function around the mode rational surface $r = r_0$ as $\phi(r,\theta) = \exp(im_0\theta)\sum_j \phi_j(r)\exp(ij\theta)$, where the toroidal and poloidal mode number (n, m_0) satisfies $q(r_0) = m_0/n$. Furthermore, we rewrite the amplitude $\phi_j(r)$ as

$$\phi_j(x,t) = A(x)\phi_0(x, t-j)\exp(ij\theta_0) \quad , \tag{2}$$

where $x \equiv n(\partial q/\partial r)_{r_0}(r-r_0) = k_\theta \hat{s}(r_0)(r-r_0)$ denotes the lowest order variation due to magnetic shear. Here, $\phi_0(t-j)$ is the zeroth order eigen-function which has a ballooning symmetry, and the corresponding eigen-value $\omega \equiv \omega_r + i\gamma$ is determined. The 2D structure is then obtained by finding the appropriate envelope function $A(x)$ and the phase shift θ_0 between adjacent rational surfaces referred to the "*Bloch angle*". $A(x)$ and θ_0 are determined by solving a global dispersion relation of order x/n so that the obtained eigen-function is well localized in the radial direction.

If we apply the above argument to the electrostatic drift wave where the eigen-frequency is given by $\omega_r(\theta_0, t) \simeq \omega_r(r_0) - \omega_r'(r_0)x$, assuming a linear pressure profile around $r = r_0$ and $\gamma(\theta_0, x) = \hat{\gamma}_0 \cos\theta_0$ from the 1D ballooning theory, we obtain the envelope function as follows :

$$A(x) \equiv \exp\left[-\frac{(\partial\omega_r/\partial x + \partial\omega_f/\partial x)}{2\hat{\gamma}_0 \sin\theta_0}x^2\right] = \exp\left[-\frac{k_\theta \hat{s}}{2\hat{\gamma}_0\sin\theta_0}\left(\frac{\partial\omega_r}{\partial r} + \frac{\partial\omega_f}{\partial r}\right)r^2\right] \quad , \tag{3}$$

where $\omega_f \equiv k_\theta V_\theta + k_\varphi V_\varphi$ is the doppler shift frequency due to plasma rotation, and (V_θ, V_φ) are the poloidal and toroidal rotation velocity where the diamagnetic component is excluded. The nonlocal mode (rm) width Δr is then given by

$$\Delta r \simeq \left|\frac{2\hat{\gamma}_0\sin\theta_0}{k_\theta\hat{s}(\partial\omega_r/\partial r + \partial\omega_f/\partial r)}\right|^{1/2} = \frac{(\Delta r)_{rm}}{\left|1 + \omega_f'/\omega_r'\right|^{1/2}} \quad , \tag{4}$$

where "$\prime$" denotes the derivative with respect to "r", and $(\Delta r)_{rm} \simeq |2\hat{\gamma}_0\sin\theta_0/k_\theta\hat{s}\omega_r'|^{1/2}$ is the mode width in the absence of plasma rotation (i.e. $\partial\omega_f/\partial r = 0$). The Bloch angle θ_0 is determined so that the wave function Eq.(3) is well localized in the radial direction. The condition is first given as $-\pi < \theta_0 < 0$ for $\hat{s}(\omega_r' + \omega_f') > 0$ and $0 < \theta_0 < \pi$ for $\hat{s}(\omega_r' + \omega_f') < 0$. Since the rapid decay of the envelope happens when $\theta_0 \to 0$, the growth rate near $\theta_0 \simeq 0$ is given by $\gamma \simeq \hat{\gamma}_0(\cos\theta_0 - \delta/\sin\theta_0)$ and $\delta \equiv (\partial\omega_r/\partial x)/2\hat{\gamma}_0 = \omega_r'/2k_\theta\hat{s}\hat{\gamma}_0$. Taking the derivative, we see that the maximum growth rate occurs roughly at

$$(\theta_0)_{max} \simeq \mp\left|\frac{(\partial\omega_r/\partial r + \partial\omega_f/\partial r)}{2k_\theta\hat{\gamma}_0\hat{s}}\right|^{1/3} = \mp(\theta_0)_{rm}\left|1 + \frac{\omega_f'}{\omega_r'}\right|^{1/3} \quad , \tag{5}$$

where $(\theta_0)_{rm} \simeq |(\partial\omega_r/\partial r)/2\hat{\gamma}_0 k_\theta \hat{s}|^{1/3}$ is also the Bloch angle in the case of $\partial\omega_f/\partial r = 0$. The $\mp$ sign in Eqs.(4) and (5) corresponds to the cases $\hat{s}(\omega_r' + \omega_f') > 0$ and $\hat{s}(\omega_r' + \omega_f') < 0$, respectively. Note here that the corresponding growth rate is given by $\gamma \simeq \hat{\gamma}_0\cos(\theta_0)_{max}$, which is smaller than that obtained from the local analysis, $\hat{\gamma}_0$. The stabilizing effect comes from the spatial inhomogeneity of plasma equilibrium (or precisely speaking, the effect of the finite diamagnetic shear $\partial\omega_r/\partial r \sim \partial\omega_d/\partial r \neq 0$, where $\omega_d \equiv k_\theta\rho_i V_i/R_0$ is the magnetic drift frequency). Here, we describe some important properties deduced from Eqs. (4) and (5).

(I). In the absence of plasma flow shear ($\partial\omega_f'/\partial r = 0$), the 2D structure is characterized by the two parameters (Δr, θ_0) as shown in Fig.1 (a), which are approximately given by $\Delta r \propto |L_T\rho_i/\hat{s}|^{1/2}$ and $(\theta_0)_{max} \propto \mp|1/\hat{s}n|^{1/3}$. Here, we have simply used the relation $\partial\omega_r/\partial r \simeq \omega_d/L_T$ ($L_T \equiv |d\ln T_i/dr|^{-1}$), and $\hat{\gamma}_0 \sim \omega_r \sim \omega_d$. This shows an existence of the radially extended nonlocal mode as already discussed in Eq.(1). Here, θ_0, corresponds to a "tilting angle" of the nonlocal mode from the mid-plane ($\theta_0 = 0$). The result shows that when the magnetic shear becomes weak, although the mode width is extended as shown in Fig.1 (c), the tilting angle increases, and then the growth rate is expected to decrease according to the relation $\gamma \simeq \hat{\gamma}_0\cos(\theta_0)_{max}$.

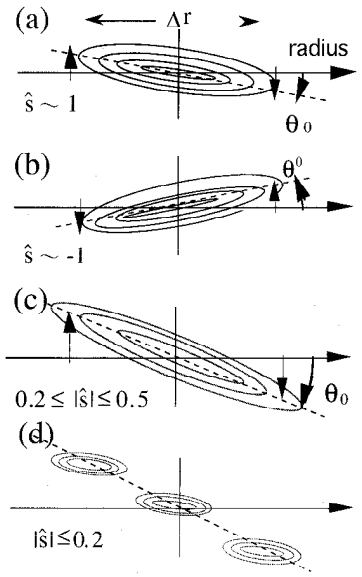

Figure 1: Shematic Picture of 2-dimensional drift wave stucture in each strength of magnetic shear.

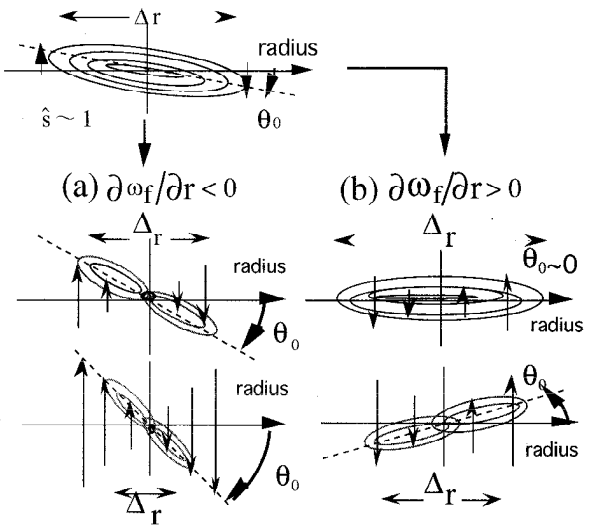

Figure 2: Schematic picture of 2-dimensional drift wave structure in the presence of plasma shear flow. (a) is the case where the direction of shear flow is the same direction as that of diamagnetic shear rotation and (b) is the opposite case.

(II). From Eqs.(4) and (5), it is found that the shear flow plays a similar role as that of the diamagnetic shear as shown in Fig.2. From Eq.(5), when the plasma flow shear is applied in the same direction as that of diamagnetic shear (i.e. $\omega_r' < 0$ and $\omega_f' < 0$), the tilting angle increases in the negative direction [see Fig.2 (a)], so that an asymmetry of the mode is enhanced and the growth rate is reduced. On the other hand, when the flow shear is applied in the opposite direction to that of the diamagnetic shear ($\omega_r' < 0$ but $\omega_f' > 0$) [see Fig.2 (b)], the initial tilted angle $\theta_0 < 0$ is once corrected as $\theta_0 \simeq 0$ and/or $1 + \omega_f'/\omega_r' \simeq 0$, so that the symmetry of the mode structure is recovered and the growth rate is increased. Namely, the effect of the diamagnetic shear is cancelled by that of the flow shear. When the flow shear is strong enough as that $1+\omega_f'/\omega_r' < 0$, the mode is tilted in the positive direction and the growth rate once more decreases. Note that the sign of the tilting angle is changed depending on that of the magnetic shear as shown in Fig.1(a) and (b) and this is essential in forming a transport barrier as we discuss later. These dependences have been numerically investigated [2,6].

(III). The toroidal mode is stabilized when the flow shear makes $|\theta_0| \sim \pi/2$ or $|\delta| \equiv (\omega_r' + \omega_f')/2k_\theta \hat{s}\hat{\gamma}_0 \sim 1$ and this leads to the condition for stabilizing the toroidal modes from Eq.(5):

$$\gamma_0 \sim \frac{1}{2k_\theta \hat{s}} \left| \frac{\partial \omega_r}{\partial r} + \frac{\partial \omega_f}{\partial r} \right| \simeq \frac{1}{2\hat{s}} \left| -\frac{\omega_d}{(k_\theta \rho_i)} \left(\frac{\rho_i}{L_T} \right) + \left\{ \frac{V_\theta}{L_\theta} + \left(\frac{k_\varphi}{k_\theta} \right) \frac{V_\varphi}{L_\varphi} \right\} \right| , \tag{6}$$

where the last term is estimated by introducing the scale length of poloidal and toroidal flow, $L_\theta \equiv (\partial \ln V_\theta/\partial r)^{-1}$ and $L_\varphi \equiv (\partial \ln V_\varphi/\partial r)^{-1}$, and $k_\phi/k_\theta = r/R_0 q$. Here, L_θ and L_φ have a sign. We note that the stabilizing effect is inversely proportional to the magnetic shear $\hat{s}$, so the flow shear effect is enhanced in the weak magnetic shear region. If we neglect the diamagnetic shear term, the relation becomes $\gamma_0 \sim |\partial \omega_r/\partial r|/2k_\theta \hat{s}$. The stability condition of Eq.(6) which results from the linear, but nonlocal analysis might be compared with the shearing rate by Hahm and Burrell [7,8] which is derived from the nonlinear decorrelation for the flute-like modes.

2.2 Simulation study of magnetic shear dependence on "nonlocal modes"

We investigate the above theory by a toroidal particle simulation. In the simulation, full kinetic ions and adiabatic electrons are employed. The ion temperature is initially given by an *arctan-*

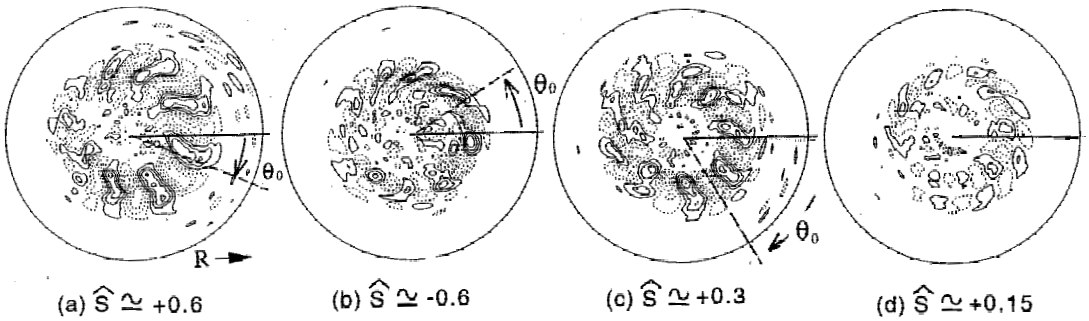

Figure 3: Potenial structure in poloidal cross section for the linear q-profile: (a) normal shear, (b) negative shear, (c) normal, but weak shear, and (d) extremely weak shear case.

profile [Fig.5(c)] and the density is almost flat to simulate a typical ITG mode. Basic parameters are $< \rho_i > /a \simeq 0.01$, $R_0/a = 0.325$, and $< T_e/T_i >= 1$ ($<>$: volume average), and the maximum pressure gradient $\bar{r}_*(\equiv r_*/a)$ locates around $\bar{r}_* \simeq 0.4$. The temperature gradient is chosen to be favorable for excitation of the ITG mode.

Here, we employ a linear q-profile by changing the gradient for three different cases; (a) normal shear case with $\hat{s} \simeq 0.6$ around $r = r_*$, (b) negative shear case with $\hat{s} \simeq -0.6$, (c) normal but weak shear case with $\hat{s} \simeq +0.3$, and (d) extremely weak normal shear case $\hat{s} \simeq +0.15$. In Fig. 3, the contours of the electrostatic potential in (r, θ) poloidal cross section are shown in the linear stage before saturation. It is shown in Fig. 3(a) that typical nonlocal modes which have a prominent ballooning structure are observed. The poloidal angle which gives the maximum growth rate is shifted to the negative direction ($\theta_0 < 0$), but when the magnetic shear is reversed, the angle shifts to the positive direction ($\theta_0 > 0$). These are consistent with the theory. When the magnetic shear is further decreased [Fig. 3(c)], the tilted angle increases in the negative poloidal direction, but the radial structure is maintained. In the extremely weak shear case, the nonlocal modes are hardly sustained and found to disintegrate as shown in Fig.3(d).

3 Drift waves in reversed magnetic shear configuration

In this section, we investigate how the toroidal modes behave in reversed magnetic shear configurations based on the theory in Sec.2. Here, we model the reversed shear plasma by choosing a parabolic q-profile as shown in Fig. 4(a), which has a q_{min}-surface inside the plasma column. Note that for the toroidal mode number n, the poloidal harmonic given by $j = m_0$ has two rational surfaces around $r = r_{min}$, but no rational surface for the harmonics with $j \leq m_0 - 1$, satisfying $(m_0 - 1)/n < q_{min}$. This means that it is no longer possible to have the wave function form $\phi_j = \phi_0(t - j)$ [ballooning symmetry : see Eq.(2)] for the mode with $j \leq m_0 - 1$. Therefore, toroidal coupling becomes difficult below $m_0 - 1$ and will result in the rapid decay of the amplitude of the corresponding poloidal harmonics [Fig. 4(a)]. Then, it is expected that the nonlocal modes are hardly excited around the q_{min}-surface and there occurs a *discontinuity* and/or *gap* at the minimum q_{min}-surface in the global mode structure.

We here utilize the Bloch angle argument in Sec.2. Since the q-profile is reversed at $r = r_{min}$, the Bloch angle has an opposite sign for the inside and outside modes with $\theta_0^{(in)} > 0$ and $\theta_0^{(out)} < 0$ as schematically shown in Fig.4(b). This leads to a *slippage* in the poloidal phases given by $\Delta\theta_0 = |\theta_0^{(in)} - \theta_0^{(out)}|$. When the slippage angle $\Delta\theta_0$ becomes of order unity [i.e. $\Delta\theta_0 \simeq O(1)$], the formation of a global wave across the q_{min}-surface is greatly reduced due to the substantial phase mismatch. We note that the slippage angle is a function not only of the magnetic shear, but also of the plasma shear rotation as discussed in Sec.2. Thus, we can simply estimate the condition to have a discontinuity from Eq.(5) :

$$|\Delta\theta_0| \sim 2|\theta_0^{(in)}| \sim 2\left|\frac{(\partial\omega_r/\partial r + \partial\omega_f/\partial r)}{2k_\theta\hat{\gamma}_0\hat{s}}\right|^{1/3} \sim O(1) \quad . \tag{7}$$

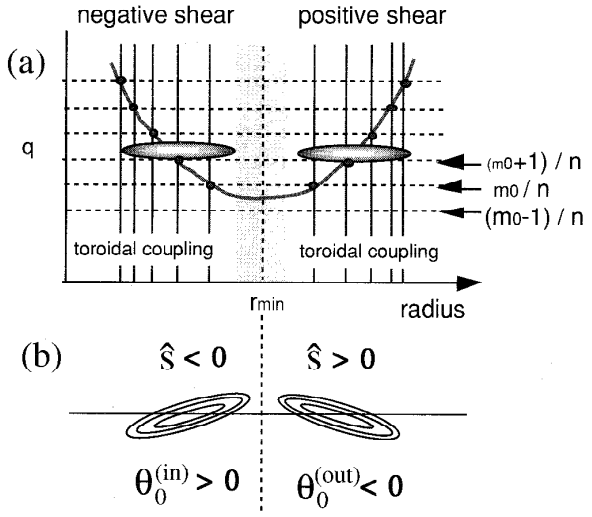

Figure 4: Relation between a reversed q-profile and corresponding mode rational surface distribution. For given toroidal number n, the mode m0 has two rational surfaces, but the mode m0-1 is non-resonant.

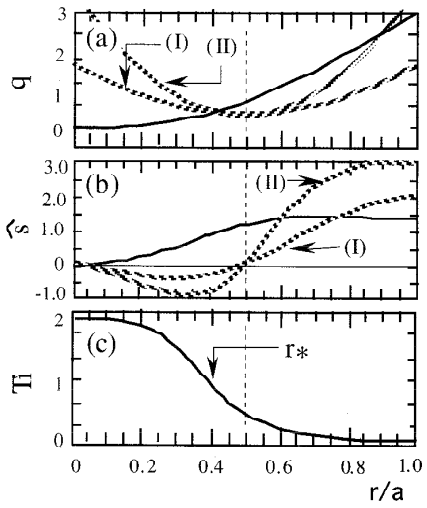

Figure 5: Radial variation of (a) safety facor q(r),(b) magnetic shear s, and (c) ion temperature. The maximum pressure gradient correspond to r*.

Here, the magnetic shear is estimated by expanding the q-profile around the q_{min}-surface as $\hat{s} \simeq (2c_1\bar{r}_m^2/q_m)(\bar{r}-\bar{r_m}) \sim 2c_1\bar{r}_m^2(L_T\rho_i)^{1/2}/q_m r_m$, assuming $|r-r_m| \sim (L_T\rho_i)^{1/2}$.

4 Toroidal Simulation in Reversed q-profile

In order to investigate the formation of the discontinuity and the related transport barrier, we perform the troidal simulations in reversed q-profile. In sec. 4.1, we present the self-consistent simulation which includes the $(m,n) = (0,0)$ component. In sec.4.2, we show the case where the radial electric field is externally applied by removing the $(0,0)$-mode from the simulation.

4.1 self-consistent simulation with (0,0)-mode

In the simulation, the q-profile is chosen as $q(r) = q_{min} + c_1(\bar{r}-\bar{r}_{min})^2$, where $\bar{r} = r/a$ and $\bar{r}_{min} = r_{min}/a$ [profile (I) in Fig. 5(a) and (b)]. The pressure profile is the same as the one used in Fig. 3 and the q_{min}-surface is chosen so that it is located outside the maximum pressure gradient surface as $r_* < r_{min}$. Note that this positional relation is generally observed in the JT-60U reversed shear experiments [9].

In Fig. 6, we show three different snap shots of electrostatic potential for the q-profile of (I) in Fig. 5(a) and (b) [parameters are $c_1 = 4.14$, $\bar{r}_{min} = 0.5$ and $q_{min} = 0.888$]. As seen in Fig.6, the ITG modes are first excited inside the q_{min}-surface and this results from the steep pressure gradient in the negative shear region [Fig.6(a)]. The heat flux induced by the waves advances to the q_{min}-surface. Then, due to the weak toroidal coupling, the waves are partially damped so

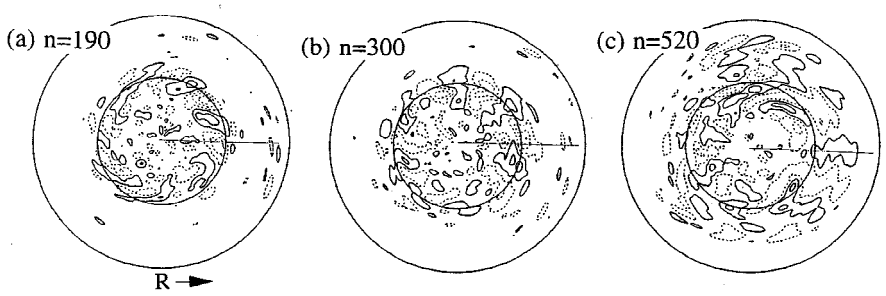

Figure 6: Potential structure in poloidal cross section at three different time steps for a reveresed q-profile in (I) in Fig.5, i.e. weak curvature case at q-minimum case.

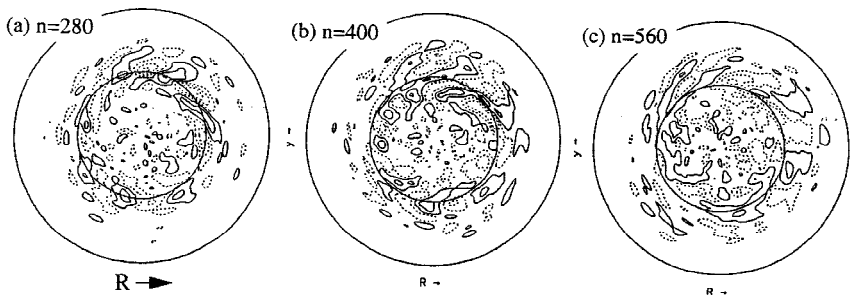

Figure 7: Potential structure in poloidal cross section at three different time steps for a reveresed q-profile in (I-I) in Fig.5, i.e. strong curvature case at q-minimum case.

that the heat is prevented to corss the q_{min}-surface. However, the damping is not enough, and as seen in Fig.6(b), some waves are excited around $r = r_{min}$ and a part of the heat is ejected from the inside region to the outside. In later time [Fig.6(c)], although the ITG modes are excited in the overall region, the phase relation between the inside and outside modes is disconnected, suggesting the existence of a *discontinuity* and/or *gap* in the phase as we discussed in Sec.3. Outside the q_{min}-surface, the waves with a long radial correlation length are observed. This is a result of the weak magnetic shear and the long scale length of the temperature profile, as predicted from Eq.(4).

Figure 7 shows similar snapshots to Fig.6, but the curvature of the q-profile at the q_{min}-surface is increased by choosing $c_1 = 10.9$ with the same $\bar{r}_{min}$ and q_{min} values [profile (II) in Fig. 5(a) and (b)]. The ITG modes are excited both inside and outside the q_{min}-surface. In this case, however, the inside and outside regions are coupled and radially extended modes occur across the q_{min}-surface. Once these kind of modes are excited across the q_{min}-surface, the heat is also ejected and the temperature profile rapidly relaxes. In the quasi-steady state, the waves across the q_{min}-surface disappear and the discontinuity is once more recovered. The excited modes that appear across the q_{min}-surface are considered to be from a different type of eigen-function which does not result from the usual toroidal coupling.

4.2 Simulation with externally driven shear flow

In order to have a discontinuity which works well as a transpont barrier, the waves excited around the q_{min}-surface as seen in Fig. 7(a) must be suppressed. The self-generated radial electric field is included in these simulations, but the resulting zonal flow shear is not strong enough to suppress these waves. Therefore, in order to investigate the effect of plasma shear flow on the discontinuity formation, we turned off the $(m, n) = (0, 0)$ mode in the simulation and externally imposed the radial electric field shown in Fig.8(a), with resulting poloidal shear flow given by $V_\theta(r) = cE_r(r)/B$ (where the toroidal field is chosen to be $\mathbf{B} = -B\hat{\varphi}$).

The direction of the shear flow is same to that of diamagnetic shear ($\omega_r'/\omega_f' > 0$) for the case (I) (solid line in Fig.8(a)) around the q_{min}-surface, but opposite ($\omega_r'/\omega_f' < 0$) for the case (II) (dotted line in Fig.8(a)). Note that the case (I) and (II) correspond to Fig.2(a) and (b), respectively. Figure 9 shows snapshots for the case (I). The mode excited inside the q_{min}-surface was seen to be damped around the q_{min}-surface [Fig.9 (a) and (b)], and in later time, a clear discontinuity was observed as seen in Fig.9 (c). Since the heat flux is dammed up near the discontinuity, the temperature profile becomes steeper around the q_{min}-surface as seen in the dashed line in Fig. 8(b), showing the emergence of transport barrier. On the other hand, Fig.10(a) shows the snapshot for the case (II). As seen in the figure, the discontinuity is weakened (or it disappeared) so that the mode is excited across the q_{min}-surface. This is due to the fact that the effect of diamagnetic shear is cancelled by the flow shear as discussed in Sec.2 so that the phase difference between the inside and outside modes becomes small. Figure 10(b) shows the time history of the fluctuation energy for the case (I) and (II). It is found that the fluctuations are more suppressed for the case (I) than that for the case (II), supporting the above idea. Thus, the active control of the radial E_r field is found to be efficient for the control of such a transport barrier.

The width of the gap will depend on the toroidal mode number n or the rational surface interval, becoming smaller with increasing n. When we approximate the gap width as the rational surface interval, we have $(\Delta r)_{gap} \sim (\Delta r)_{rs} \simeq 1/sk_y$. For the JT-60U discharge with

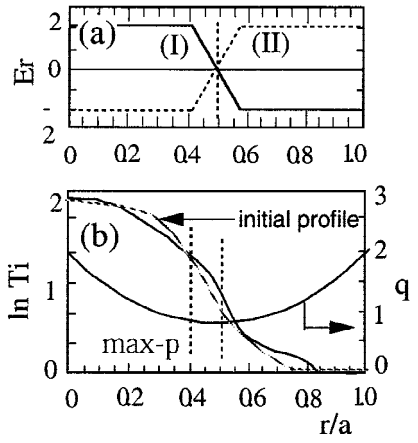

Figure 8: (a) Radial profiles of externally driven radial electric field Er employed in the toroidal simulation in Fig.9 and (10). The flow shear with different direction is applied around the q-min. surface. (b) Intial temperature profile (dashed line) and temperature profile at the quasi-steady state for the case (I) in Fig.(a). Owing to the discontinuity, steepening of the temperature profile is observed.

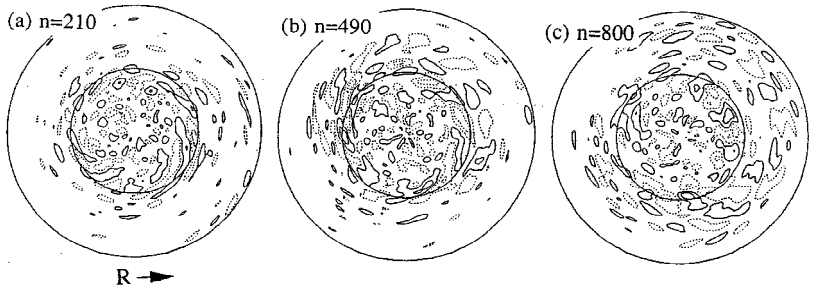

Figure 9: Potential structure in poloidal cross section at three different time steps for case (I) in Fig.8 (a)

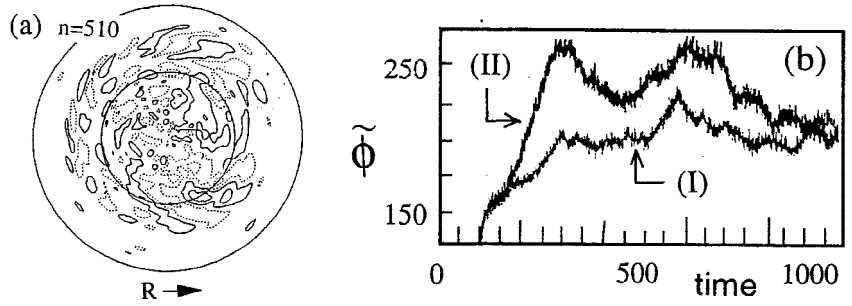

Figure 10: (a) Potential structure in poloidal cross section for the case (II) in Fig.8 (a). (b) Time history of the fluctuation energy for the case (I) and (II) in Fig.8(a), respectively.

$\rho_i \sim 0.3cm$ near the ITB, $(\Delta r)_{gap}$ provides almost the same value for the radial extent where the condition $|\hat{s}| \leq 0.22$ is satisfied. Thus, the observed discontinuity (or gap) plays a crucial role in forming the ITB near the q-minimum region, and it tends to reduce the growth rate associated with the weak/negative magnetic shear.

5 CONCLUSION

Based on the nonlocal theory, which solves the first order ballooning equation and also on the toroidal particle simulation, we investigated the drift wave structure in weak and reversed magnetic shear plasma. In these situations, since the magnetic shear becomes extremely weak or zero, the toroidal coupling which is the origin of the radially extended nonlocal modes is weakened and disappears and then the discontinuity is expected. The formation of such a discontinuity is confirmed via toroidal particle simulation and it is found that the formation sensitively depends on the magnetic structure, specifically, on the curvature of the q-profile at the q_{min}-surface.

From the simulation, weak curvature is found to be preferable to form the discontinuity, which is consistent with the theory. However, in some cases, we observed the waves which are excited across the q_{min}-surface. Once such modes are excited, the discontinuity deteriorates and heat is ejected from the inside region to the outside. Owing to this kind of mode activity, the transport sometimes becomes intermittent, repeating the formation and destruction of the discontinuity. These results suggest that the reversed magnetic shear configuration allows the

excitation of various types of eigen-modes with different linear growth rates over a finite radial region across the q_{min}-surface. Candidates for these modes are, in addition to the toroidal modes which are connected through the nonresonant mode as we discussed in Sec.3, a trapped ion mode which is insensitive to the magnetic shear and localizes at larger pressure gradient region[13], and/or a recently investigated slab mode referred to as a "global mode" or "double mode" [14]. In addition to this, whether the discontinuity is established depends on the relative positional relation between the q_{min}-surface and the maximum pressure gradient surface, and the strength and direction of the plasma shear rotation. It is also found that the discontinuity efficiently works as a thermal barrier when the q_{min}-surface is located outside the maximum pressure gradient position, which is consistent with experimental results. Furthermore, when the flow shear is applied to the same direction as that of the diamagnetic shear, the discontinuity condition is easily obtained.

Acknowledgements

We acknowledge Dr. M.Azumi and Dr. H.Kishimoto for supporting our works.

Reference

[1] Y.Kishimoto, J.Y. Kim, et.al. Proceedings of the 16th International Conference on Fusion Energy, (IAEA, Vienna, 1997) Vol.2, 581-591, 1997; also Y. Kishimoto et.al. the 25th EPS/ICPP combined conference, Prague, Czech, 1998 (June 29 -July 3), To.45, to be published in Plasma Physics and Controlled Fusion, 1999.

[2] Y.Kishimoto, T.Tajima, et.al. Phys. Plasmas 3, (1996) 1289.

[3] M.J.LeBrun, T.Tajima, et.al. Phys. Fluids, 752 (1993).

[4] S.E.Parker, W.W.Lee and R.A.Santoro, Phys. Rev. Lett. **71** 2042 (1993).

[5] J.W.Connor, J.B.Taylor and H.R.Wilson, Phys. Rev. Lett. **70** (1993) 1803, J.Y.Kim and M.Wakatani, Phys. Rev. Lett. (1994) 2200.

[6] J-Y.Kim, Y.Kishimoto, W.Horton and T.Tajima, Phys. Plasmas **3**, 3689-3695 (1996).

[7] K.H.Burrel, Phys. Plasmas **4(5)**, 1499 (1997)

[8] T.S.Hahm and K.H.Burrel, Phys. Plasmas **2**, 1648 (1995).

[9] T.Fujita et.al. Phys. Rev. Lett. **78**, 2377 (1997).

[10] W.Horton, T.Tajima, et.al. Plasma Phys. Control. Fusion **39**, 83 (1997).

[11] Shirai and the JT-60 Team, Phys. Plasmas **5**, 1712 (1998).

[12] F.Romanelli and F.Zonca, Phys. Fluids **B5**, 4081 (1993).

[13] M. Artun, W.M. Tang, and G. Rewildt, Phys. Plasmas **2**, 3384 (1995).

[14] J.Q.Li, L.Huang, and W.Qu, Phys. Plasmas **5**, 959 (1998).